Damage localization in bridges via the FRF interpolation method

M. Dilena [a], M.P. Limongelli [b], A. Morassi [a,c,*]

[a] Università di Udine, Department of Civil Engineering and Architecture, Via Cotonificio 114, 33100 Udine, Italy
[b] Politecnico di Milano, Department of Architecture, Built Environment and Construction Engineering, Piazzale Leonardo da Vinci 32, 20133 Milano, Italy
[c] Department of Mechanical Engineering, Universidad Carlos III of Madrid, Avda. de la Universidad 30, 28911 Leganés, Madrid, Spain

Received 25 January 2014
Received in revised form
28 June 2014
Accepted 8 August 2014
Available online 1 September 2014

1. Introduction

The identification of damage in a bridge from changes in its vibrational behavior is an inverse problem of important practical value. Every structural health monitoring program must necessarily deal with this issue in order to provide quantitative estimates of the level of residual safety.

Significant advances have been obtained on this topic in the last two-three decades, both from the theoretical and applied point of view. Without claim of completeness, here we recall the investigations developed by Toksoy and Aktan [1], Teughels and De Roeck [2], Cruz and Salgado [3], Necati Catbas et al. [4], Magalhaes et al. [5]. A critical review of the literature shows that there is still no general consensus among the experts of the field on the type of the data to be taken as good indicator of damage and also on the effectiveness of a diagnostic method rather than another. One of the reasons for this uncertainty is to be ascribed to the peculiar structural behavior of each bridge and to the lack of standard approaches to structural analysis of bridges. However, the main difficulty is due to the inverse nature of the diagnostic problem and, consequently, to the non-uniqueness in the identification of damage from dynamic measurements and to the non-continuous dependence of the solution on the data. Moreover, when identification techniques are applied to study full-scale real bridges, additional obstacles arise due to the small sensitivity of the dynamic parameters to damage, the presence of error in measurements and the incompleteness of the field data. The effect of environmental changes could make

* Corresponding author at: Università di Udine, Department of Civil Engineering and Architecture, Via Cotonificio 114, 33100 Udine, Italy.
Tel.: +39 0432 558739; fax: +39 0432 558700.
E-mail addresses: michele_dilena@email.it (M. Dilena), mariapina.limongelli@polimi.it (M.P. Limongelli), antonino.morassi@uniud.it (A. Morassi).

identification even less reliable in some cases. It is probably because of these difficulties that, so far, a limited number of studies have investigated the effect of damage on the dynamic behavior of full-scale bridges and developed suitable strategies for damage identification. In this connection, we recall, among others, the research developed by Kato and Shimada [6], Farrar and Jauregui [7], Maeck et al. [8], Dilena and Morassi [9].

A class of diagnostic methods is based on the interpretation of changes in modal parameters (typically, natural frequencies and mode shape amplitudes) produced by the damage. From these investigations it emerges that damage-induced changes in natural frequencies generally are measurable, see, for example, [6,10]. However, their use for damage detection purposes in bridges should be consider with caution, since several researchers have shown that natural frequencies could not reliably identify location and the level of damage, see, for instance, [1,7]. The main reason is that, in order to extract quantitative information on damage from natural frequencies only, an accurate mechanical model of the system and of the damage mechanism must be available, and this is not the case in many practical applications on bridges, see, as an example, the research developed in [11]. From several studies it turns out that, in spite of the fact that measurement of modal amplitude estimates are typically affected by errors larger than those affecting natural frequencies, mode shapes are the best indicator of where the damage is occurring, see, for example, [10,12]. Mode shape data, actually, contains direct information of the spatial character of the structural change, even if their ability to identify damage seems to require the application of suitable identification strategies. Mode shapes, in conjunction with the corresponding natural frequencies, have been used in [1,13] to reconstruct the flexibility matrix of a bridge. The change in the stiffness coefficient caused by the damage is determined via model updating procedures in [2] so that a given set of natural frequencies and corresponding mode shapes are close in some least square sense to those found experimentally. Other methods focus on the determination of mode shapes or their derivatives to localize damage. The Modal Curvature Method (MCM), proposed by Pandey et al. [14] on cracked beams, has been applied to bridges by Wahab and De Roeck in [15]. Modal curvature has been shown to be more sensitive to damage than modal shapes, allowing a more effective identification of structural change when the damage is localized and one-dimensional beam behavior is dominant on the bridge response. The drawback of the MCM is mainly connected with the need of evaluating the second derivative of the mode shape in presence of noise on the data. However, it was shown in [9] that a suitable spline interpolation of the measured data can lead to correct identification of the damage even in presence of few measurement points, provided that accurate estimates of the modal parameters are available. In connection with this aspect, it should be recalled that a lot of research has pointed out that there are situations in which modal parameters are sensitive to changes in environmental conditions (temperature, moisture, loading), and these effects should taken into account in order to obtain a correct damage reconstruction, see, for instance, [16].

Another approach to damage identification in bridges that does not need the estimation of modal parameters nor a numerical model of the structure - since it works directly on the experimental data—has been proposed in recent years. A class of methods is based on a definition of a damage index in terms of variations of the Operational Deformed Shapes (ODSs) calculated from frequency response functions in the inspection phase with respect to a reference state. An ‘operational deformed shape’ is the deflection shape of a structure subjected to harmonic excitation. If the frequency of the excitation is close to a modal one, the ODS is dominated by the corresponding mode shape; for other values of the frequency of excitation the ODS derives from the combination of several modes.

Abrupt changes of the ODS are interpreted as a symptom of a stiffness loss due to a localized damage. The Frequency Response Curvature Method (FRCM), proposed by Sampaio et al. [17], and the Gapped Smoothing Method (GSM), proposed by Ratcliffe [18], define a damage index in terms of the variation of curvature related to the reduction of stiffness and estimated from operational deformed shapes. More recently, Ramesh Babu and Sekhar [19] developed a technique for the localization of small cracks based on a damage detecting feature called Slope Deviation Curve (SDC) calculated in terms of the slope of the operational deflection shapes.

The local reduction of smoothness in the curvature of the ODSs was proposed as a damage detecting feature also by Zhang [20] in a new damage detection algorithm called the Global Filtering Method (GFM) and based on the ODS extracted from the dynamic response of a passing vehicle excited by a sinusoidal tapping force. The drawback still connected with both these methods is that the numerical differentiation needed to evaluate slope or curvature introduces errors that often prevent the detection of damage in case of noisy data.

Methods based on the interpolation of the ODS using smooth functions to enhance the lack of smoothness at the location of damage do not require the estimation of curvature, thus overcoming some of the problems related to noise in recorded signals. Pai and Jin [21] proposed a Boundary Effect Detection (BED) method based on the use of trigonometric functions to model the ODS of a beam and of a sliding window least-square curve fitting technique to estimate the coefficients of the curve. Basing on the variations of values and sign of these coefficients along the beam, the location of damage can be detected. More recently, the Interpolation Damage Detection Method (IDDM) for damage localization recently was proposed by Limongelli [22]. The IDDM tries to overcome the drawback of using curvatures by defining a damage index in terms of deformed shapes, hence reducing errors connected with double differentiation. A spline interpolation of the deformed shapes is used to enhance the variation of the deformed shape connected to damage thus avoiding the estimation of curvatures.

In this paper the sensitivity of the IDDM is investigated with reference to the case of a reinforced concrete single-span bridge in the Municipality of Dogna (Friuli, Italy). The bridge consists of a slab supported by three longitudinal beams simply supported at the ends. Harmonically forced tests were conducted to evaluate the variation of the modal parameters of lower

vibration modes after imposing artificial, increasing levels of localized damage [9]. The sensitivity of the method is documented and discussed with respect to the amount of experimental data used and to the severity of the damage scenarios considered. Specifically, the sensitivity of the results to the number of available responses, that is the number of instrumented locations, has been investigated thanks to the availability of sensors deployed along three alignment parallel to the longitudinal direction of the bridge. Results obtained using just one of the alignments are compared to those given by the all set of available sensors. Furthermore, the availability of responses recorded before and after damage scenarios of increasing severity allowed to assess the capability of the method to localize a new damage on a structure already damaged. Finally, the sensitivity of results of the IDDM to the number of modal contribution considered in the estimation of the damage feature has been also investigated and discussed and, in order to check the reliability of results given by the IDDM, a comparison with the well-known Modal Curvature Method is presented.

2. The interpolation method for damage localization: an overview

2.1. The basis of the method

The method applied herein to identify *concentrated* damages is the Interpolation Damage Detection Method presented by Limongelli in the case of seismically excited structures [22,23]. The IDDM is based on the determination of a point-wise interpolation error connected with the approximation of a selected *vibrational amplitude profile* of the structure by a polynomial spline function. Specifically, at any given location the interpolation error is defined as the difference between the vibrational amplitude actually measured and the vibrational amplitude computed at that same location by interpolating the vibration amplitudes measured at all the other locations.

The main hypothesis underlying the method is that a concentrated damage reflects in a loss of spatial regularity of the vibrational profile of a structure, compared with the reference (undamaged) state. This actually happens in beams with a localized damage, such as notches or cracks, since the transverse displacement in the Euler–Bernoulli model loses the C^1-regularity at the damaged cross-sections (see, for example, [24]) and in thin elastic plates with inclusions [25]. Therefore, the possible increase of the interpolation error between a reference state and an inspection state at one instrumented location is considered in this method as an indicator of the occurrence of structural damage close to the location where the change has been detected.

For reader convenience, the main basis of the IDDM are briefly recalled in the sequel. In order to simplify the presentation, reference is made to a straight beam under small in-plane bending vibration and the vibrational amplitude profile is defined in terms of the frequency response function (FRF) of the acceleration. We refer to the papers [22,23] by Limongelli for a more exhaustive presentation of the method.

Let us denote by $\{z_l\}_{l=1}^{n}$ the set of instrumented points located along the beam axis z, as shown in Fig. 1. At the lth location z_l and at frequency f_i, we denote respectively by $H_R(z_l,f_i)$ and $H_S(z_l,f_i)$ the transfer function value calculated from the recorded signals and through cubic polynomial spline interpolation of the transfer functions $H_R(z_k,f_i)$ measured at all the other instrumented locations $\{z_k\}_{k=1}^{n}$, with $k \neq l$, that is

$$H_S(z,f_i) = \sum_{j=0}^{3} c_{j,l}(f_i)(z-z_{l-1})^j \quad z \in [z_{l-1}, z_l], \tag{1}$$

where the coefficients $(c_{0,l}, c_{1,l}, c_{2,l}, c_{3,l})$ are functions of the values $H_R(z_k,f_i)$ at locations $\{z_k\}_{k=1,k\neq l}^{n}$:

$$c_{j,l}(f_i) = g(H_R(z_k,f_i))\ k \neq l \tag{2}$$

The interpolation error $E(z_l f_i)$ is defined as the absolute value of the difference between recorded and interpolated FRFs

$$E(z_l f_i) = |H_R(z_l,f_i) - H_S(z_l,f_i)| \tag{3}$$

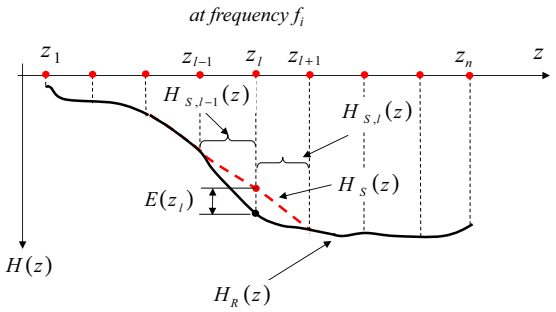

Fig. 1. Spline interpolation of the FRF at $z=z_l$. Continuous line: recorded FRF profile H_R; dashed line: interpolated FRF profile H_S.

In order to characterize each location z_l with a scalar-valued error index, the norm of the error on the whole range of frequencies is introduced

$$E(z_l) = \sqrt{\sum_{i=N_1}^{N_1+N_2} E^2(z_l, f_i)}, \tag{4}$$

where N_2 is the number of frequency lines occurring in the frequency range starting at line N_1 for which the signal-to-noise ratio is high enough to allow for a correct definition of the FRF.

Transfer function values obviously depend on the state of the structure. Hence, if the estimation of the error function through Eq. (4) is repeated in the baseline (undamaged) and in the inspection (possibly damaged) configuration, then the difference between the two values, denoted respectively by $E_0(z_l)$ and $E_d(z_l)$, can provide an indication about the existence of degradation at location z_l

$$\Delta E(z_l) = E_d(z_l) - E_0(z_l). \tag{5}$$

An increase in the interpolation error between the reference configuration and the current configuration at a station z_l, i.e. $\Delta E(z_l) > 0$, highlights a localized reduction of smoothness in the vibrational amplitude profile and, therefore, it is assumed to be a symptom of a local variation of stiffness at z_l associated with the occurrence of damage.

The above analysis has been developed in a deterministic context. Several sources, such as temperature, nonlinear behavior, soil structure interaction and noise in recorded data, can induce variations of the interpolation error even if no damage occurs. To take into account the effect of these random variations in the damage localization procedure, the statistical variability of the interpolation error $E(z_l)$ at each instrumented location $\{z_l\}_{l=1}^{n}$ should be investigated, both in the undamaged and in the inspection configurations, in order to extract and compare the relevant probability distributions $p_{E,0}(z_l)$ and $p_{E,d}(z_l)$.

If the two distributions are known, the onset of damage at a given location z_l can be investigated by checking their shift, for example in terms of the mean value. Generally, none of the two distributions is known, unless the structure is permanently monitored by a network of sensors. However, even in this case, while distribution $p_{E,0}$ at each instrumented location can be easily recovered from all the data recorded before the occurrence of damage, the estimation of $p_{E,d}$ should rely on a very small sample of values of E_d, possibly just one, if a prompt alert is required. The detection of possible damages in this case is carried out by comparing the value of E_d to the distribution $p_{E,0}$ in order to check if its value is 'likely to occur' in the undamaged configuration. Therefore, the 'possibly damaged' locations can be defined as the ones corresponding to values of the interpolation error having small probability of occurrence in the undamaged configuration, that is values that lie in the tail of the distribution $p_{E,0}$, and specifically in its upper tail since only an increase of the interpolation error is assumed to denounce damage.

In order to quantify how small the probability of occurrence must be in order to be denounce the location as 'damaged', a threshold value $E_T(z_l)$ has to be defined, so that if the value of $E(z_l)$ at a given location z_l exceeds $E_T(z_l)$ then an alarm is given about the structural condition at z_l. Actually, even if the value of $E(z_l)$ is higher than the threshold $E_T(z_l)$, there is still a (low) probability, represented by the area $P_f(z_l)$ of the squared region under the graph of $p_{E,0}(z_l)$ shown in Fig. 2, that the structure is undamaged. In this case, being the value of $E(z_l)$ beyond the threshold, an alarm is given, but it is a *false alarm* since the structure is undamaged. In addition to the probability of false alarm, the value $E_T(z_l)$ defines a value of the probability of *missing alarm* $P_m(z_l)$, that is the probability that the variation of the interpolation error is mistakenly attributed to random sources while it is actually due to a damage. If the structure is damaged but the value $E(z_l)$ is lower than the threshold, no alarm is given. In this case, there is a missing alarm since the structure is actually damaged, and the probability of missing alarm is represented by the area of the hatched region under the graph of $f_{E,d}(z_l)$ shown in Fig. 2.

From the above analysis, clearly emerges that the definition of the threshold $E_T(z_l)$ is a tradeoff between the probability of false and missing alarm. The optimal choice of the threshold basing on a cost-benefit analysis is beyond the scope of this paper and will not be performed for the application reported in the following.

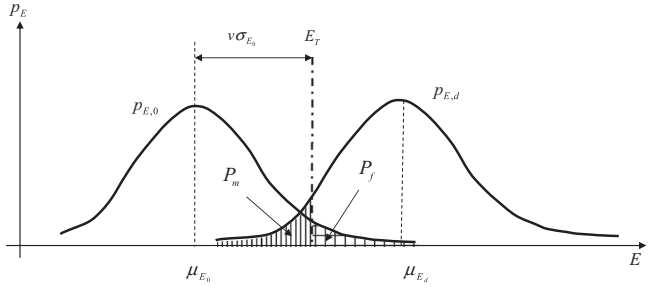

Fig. 2. Threshold and probabilities of false and missing alarm.

2.2. The damage detection procedure

The procedure described above can be implemented if the distribution of the interpolation error in the undamaged configuration is available, that is when enough data, recorded in the undamaged configuration, are available. If the structure is only occasionally or periodically tested to detect possible damages, as in most of applications and also in the present case study, the available data at each instrumented location $\{z_l\}_{l=1}^{n}$ reduce to a single estimation of $E_0(z_l)$ and $E_d(z_l)$, for the undamaged and the possible damaged structure, respectively. In this case, the lack of experimental data requires some simplifying assumptions and the application of a slightly different procedure to reduce the effect of the random variations on the interpolation error. The assumption considered herein is that all sources of random variations equally affect all the instrumented locations producing a uniform variation (uniform increase or uniform decrease) of the interpolation error at all $\{z_l\}_{l=1}^{n}$. Basing on this assumption, if a uniform variation of the interpolation error is detected, then the structure is considered undamaged and the possible variations of the interpolation error are ascribed to random sources not connected with damage. On the contrary, if the interpolation error ΔE is 'localized', namely it is 'significantly higher' at few locations with respect to the others, then a damage is denounced at those locations.

In order to select 'significant' values of ΔE, a threshold value must be introduced for this parameter in terms of its probability distribution, similarly to what previously described with reference to the case when $p_{E,0}$ is known. Assuming a normal distribution for ΔE, the threshold ΔE_T can be defined in terms of the average $\mu_{\Delta E}$ and of the variance $\sigma_{\Delta E}$ of the damage parameter $\Delta E(z_l)$ on the population of available values (that is, calculated at all the instrumented locations $\{z_l\}_{l=1}^{n}$), namely

$$\Delta E(z_l) = \mu_{\Delta E} + \nu\sigma_{\Delta E}, \tag{6}$$

being ν the value of the standard normal distribution corresponding to the threshold probability.

The damage index $D(z_l)$ at a given location $z_l$is then defined by the relation

$$D(z_l) = \Delta E(z_l) - (\mu_{\Delta E} + \nu\sigma_{\Delta E}), \quad l = 1, \ldots\ldots, n, \tag{7}$$

and positive values of $D(z_l)$ are considered as symptom of possible damage occurred at z_l. It should be recalled that if the right hand side of Eq. (7) is negative, then the damage index is assumed equal to zero. As mentioned above, an increase of ν leads to a reduction in the probability of false alarms and, simultaneously, to an increase of the probability of missing alarms. If ΔE is normally distributed, then $\nu=1$, $\nu=2$, $\nu=3$ lead to a confidence level of about 85%, 98%, 99%, respectively, that is there is 15%, 2%, 1% probability that $\Delta E(z_l)$ exceeds the threshold level and z_l be not a damage location (false alarm).

3. A case study: the Dogna bridge

In this section we describe our case study. The Dogna Bridge is the four-span, one-lane reinforced concrete bridge shown in Fig. 3. The span of the bridge highlighted in Fig. 3 has been the object of an extensive experimental/theoretical research on the use of dynamic methods for damage detection (see [9]) and structural identification of bridges (see [11]). For the sake of completeness and for reader convenience, in the sequel we briefly describe the structure and we recall the main features emerged during dynamic testing.

The bridge deck is formed by a reinforced concrete (RC) slab 0.18 m in thickness, supported by three longitudinal RC beams of rectangular cross-section $0.35 \times 1.20\ \mathrm{m}^2$. Beams are simply supported at the ends and are connected at the supports, at mid-span and at span-quarters by transverse RC diaphragms. Pier and abutments were built on cast-in-place concrete piles of 1.0 m in diameter and 18.0 m in length.

The Dogna Bridge suffered of an exceptional flood of the Fella River on August 31, 2003. A visual inspection conducted on the tested span revealed no apparent deterioration on slab and beams, whereas an advanced state of degradation was noticed on support bearings side pier. The bridge was demolished on May 2008. Dynamic tests were performed from April 2 to April 11, 2008, and during the experiments the tested span was made independent of the adjacent span by removing the deck-joint in correspondence of the pier.

Harmonically forced vibration tests were performed on the bridge in its present condition (undamaged configuration, indicated by U in what follows) and in seven damaged configurations $D1$–$D7$, see Fig. 4. The first six damage states were

Fig. 3. General view of the Dogna Bridge (left, tested span circled) and detail of damages D1–D6 (right).

obtained by cutting the downstream lateral beam. Notches were produced by using a hydraulic saw fitted with a diamond disc. The seventh level of damage was obtained by removing the concrete near the mid-span cross-section of the same beam by means of a jackhammer. The experimental layout is shown in Fig. 5 and we refer to [9] for a complete account of the experiment. The vertical motions of the deck structure were produced by means of a vibration generator consisting of a closed-loop electro-mechanic actuator mounted in vertical direction. During the experiments a time harmonic force with maximum amplitude of 15 kN has been used. Based on this experimental setup, deck's inertance of the bridge was

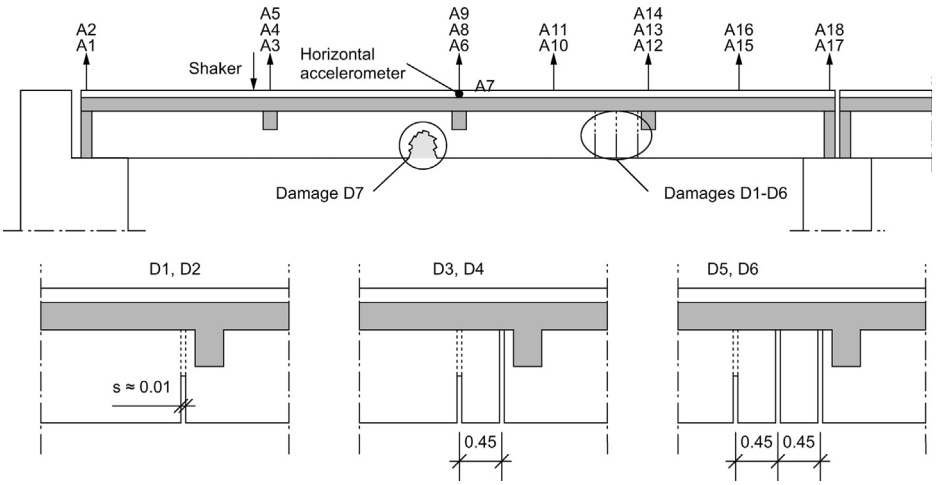

Fig. 4. Damaged configurations. Dimensions are in meters.

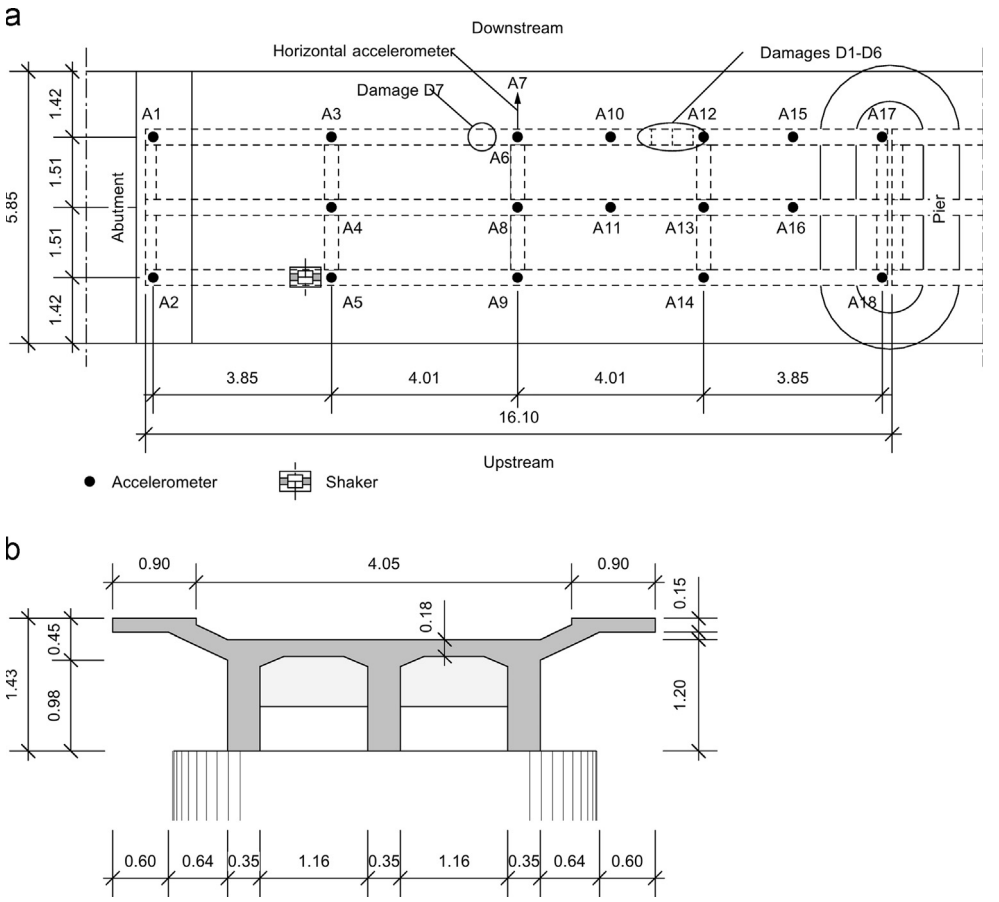

Fig. 5. Basic dimensions and instrumental layout. Dimensions are in meters.

measured by means of zoom analyses within narrow neighborhoods (approximately 3–5 Hz in size) of the natural frequencies. Frequency resolution ranged from 0.02 for the lower modes (up to 15 Hz) to 0.04 Hz for higher modes. The above procedure has been applied for the characterization of all the damaged configurations *D*1–*D*7.

By way of example, Fig. 6 shows the FRF modulus of the bridge in the undamaged and in damaged configurations *D*2, *D*4, *D*6 at locations A10, A11 and A14. In this figure, a linear interpolation of the measured FRFs has been adopted for frequency ranges in which experimental data were not available.

Fig. 7 shows the evolution of the first five natural frequencies with respect to damage. We refer to the analysis developed in [11] for a justification of the not monotonic behavior of the frequency values with respect to increasing levels of damage.

Experimental vibrating modes have dominant vertical components. As an example, the undamaged and damaged *D*4 mode shapes of the deck are shown in Fig. 8. Experimental results confirm that mode shapes are sensitive to the introduction of damage. Generally speaking, the variations are appreciable in the configuration *D*1 and become clearly measurable in subsequent damaged configurations. From visual comparison it emerges that the third and fourth modes are the most sensitive to damage and, in general, they show an increase in modal amplitude near the damaged region, see [11] for a detailed analysis.

4. Damage localization

4.1. Application of the Interpolation Damage Detection Method

As recalled in Section 3, harmonically forced dynamic tests were produced on the Dogna Bridge by a shaker located at one-fourth of the upstream beam. At the time the tests were performed, the main aim was to carry out a modal characterization of the structure, hence response were measured only within narrow neighborhoods of the expected natural frequency values (see Fig. 6). Furthermore, the size of these neighborhoods was slightly adjusted during the tests for the various damage configurations in order to match with the current natural frequency values. The FRFs at instrumented locations are thus available only in narrow frequency intervals, and the size of these intervals changes from one test to the other. The application of the IDDM requires that the values of the FRFs are defined in the same frequency interval for both the reference and the damaged configuration. Therefore, in order to calculate the FRFs in the frequency ranges where they

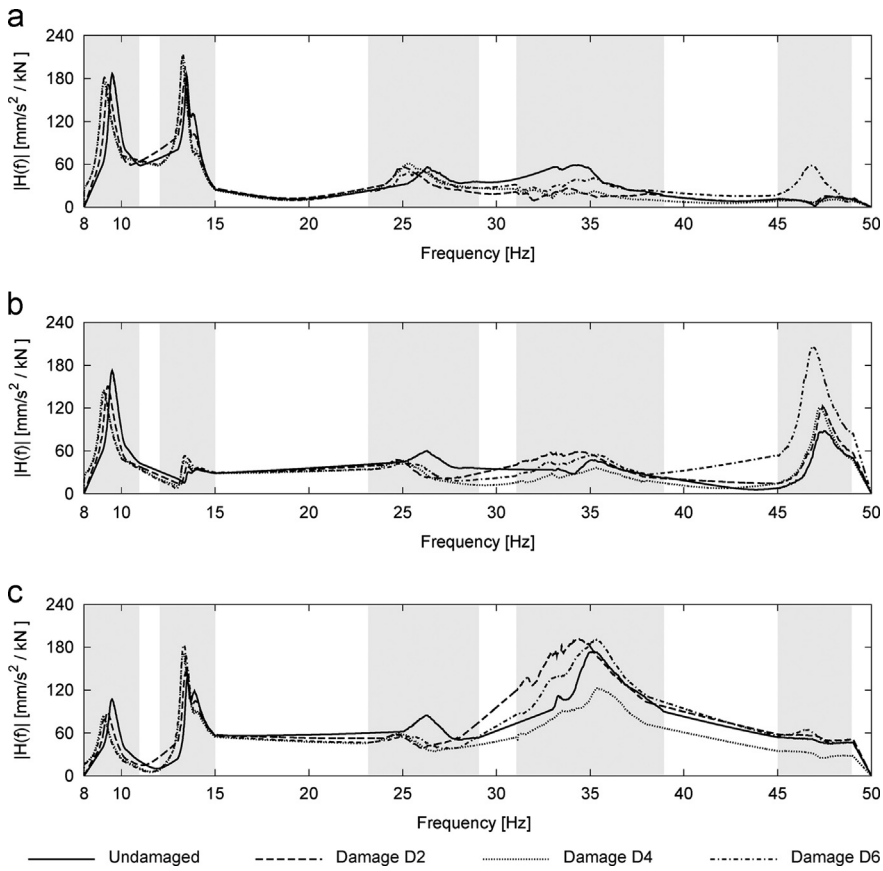

Fig. 6. FRF amplitude at locations A10 (a), A11 (b) and A14 (c) obtained by linear interpolation outside the measured intervals (in gray).

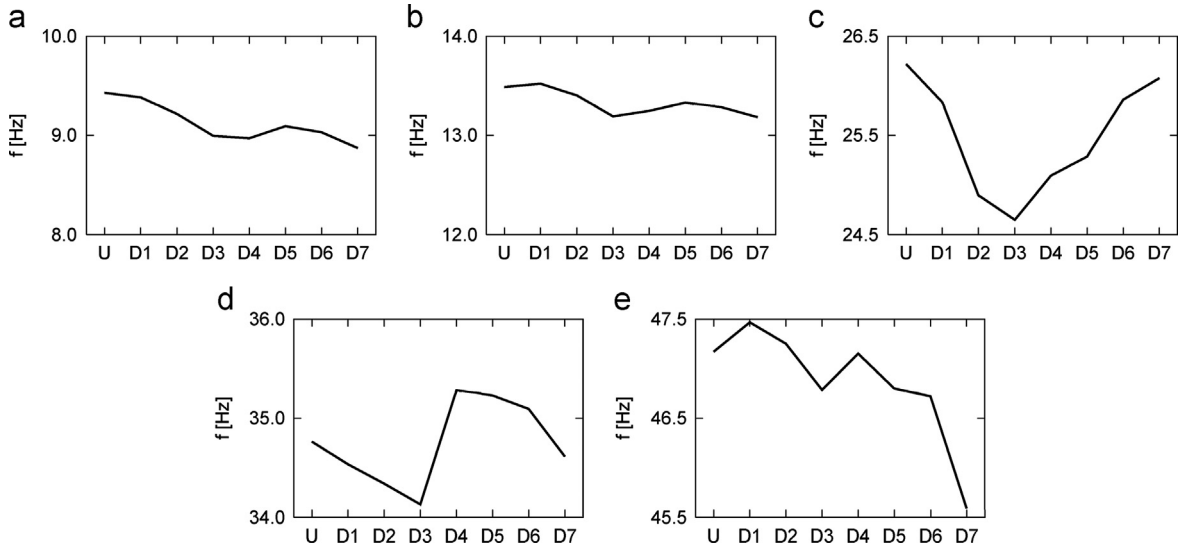

Fig. 7. Experimental natural frequency values vs damage: (a) Mode 1; (b) Mode 2; (c) Mode; 3; (d) Mode 4; and (e) Mode 5.

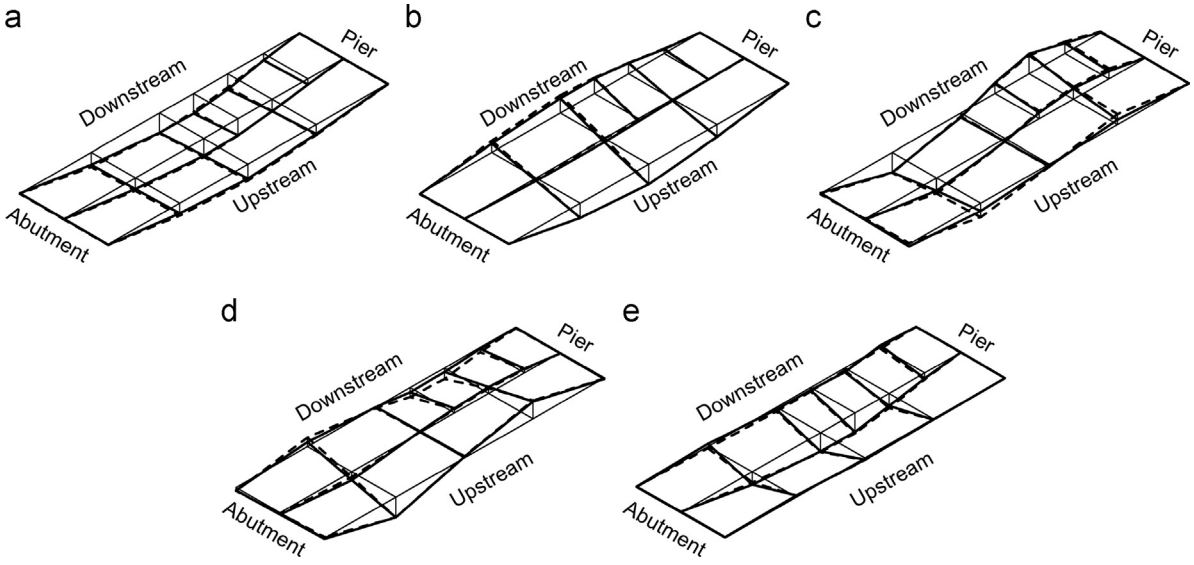

Fig. 8. Mass-normalized mode shapes in undamaged (dashed line) and damaged D4 (continuous line) configurations.

were not available, a linear interpolation of the measured values was carried out in the whole interval 8–50 Hz. Even if this choice may represent a rather crude estimation of the actual values of the FRFs outside the measured intervals, the results of the analysis show that it allows for a correct localization of the damage. The scarce influence on identification results produced by this estimation of the FRFs may be due to the fact that linear interpolation is restricted to frequency ranges which are generally far from resonance regions and that, consequently, have much lower influence on the value of the damage index with respect to near-resonance values, for all configurations considered in testing.

In order to investigate on the sensitivity of the diagnostic method to the amount of experimental data available, in a first stage the IDDM was applied considering separately the three alignment of sensors at downstream, central axis and upstream, corresponding to the set of sensors A1–A3–A6–A10–A12–A15–A17, A4–A8-A11–A13–A16, A2–A5–A9–A14–A18, respectively. More explicitly, for each alignment the damage index at an instrumented point was evaluated by considering the FRFs measured at sensors belonging to that alignment, and neglecting all the other instrumented points. Moreover, the method was implemented by considering different frequency intervals including the first two, three, four and five resonant frequencies for damage configurations *D*1–*D*7.

A preliminary analysis has been developed with the aim of estimating a suitable value of the threshold parameter ν (see Eqs. (6) and (7)). Numerical results for $\nu=2$ when the first two and the first five vibrating modes are taken into account are

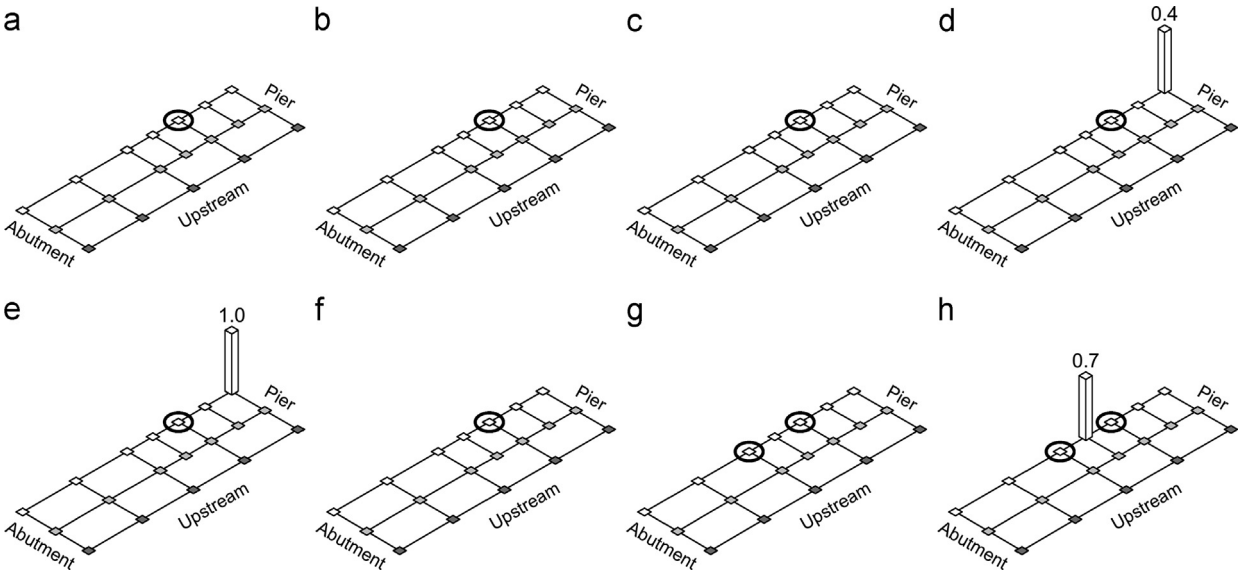

Fig. 9. Damage index D evaluated in the interval 8–15 Hz (first two vibrating modes) from the reference configuration (U) to actual damage configuration: (a) $D1$; (b) $D2$; (c) $D3$; (d) $D4$; (e) $D5$; (f) $D6$; (g) $D7$; (h) from $D6$ to $D7$. Threshold $\nu=2$. Circles denote the actual damage locations.

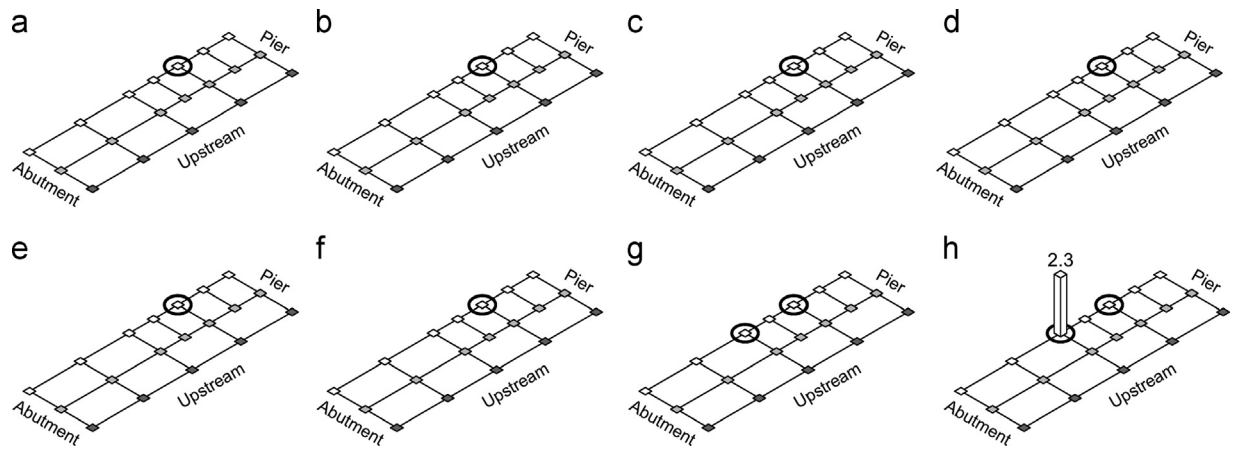

Fig. 10. Damage index D evaluated in the interval 8–50 Hz (first five vibrating modes) from the reference configuration (U) to actual damage configuration: (a) $D1$; (b) $D2$; (c) $D3$; (d) $D4$; (e) $D5$; (f) $D6$; (g) $D7$; (h) from $D6$ to $D7$. Threshold $\nu=2$. Circles denote the actual damage locations.

summarized in Figs. 9 and 10, respectively. White, light gray and dark gray columns are used throughout the figures of the paper to denote instrumented points belonging to the downstream, central and upstream beam, respectively. The height of these columns is proportional to the corresponding damage index value. The choice $\nu=2$ allows for a correct localization of severe damage only and, in addition, the probability of missing alarms turns out to be very high. Figs. 11–14 show the values of the damage index calculated with $\nu=1$. This last choice leads to a better compromise between the probability of having false and missing alarms and, unless otherwise specified, will be retained in the remaining of this section. It can be seen that, apart from few exceptions, the damage index exhibits the highest value at locations close to the actual position of damage for all the cases examined and, moreover, its value generally increases with the number of vibrating modes considered in the analysis, thus improving the localization of the damage. This behavior is particularly evident when the values obtained using the first two modes only are compared with those calculated by adding the third mode, see Figs. 11 and 12. The analysis also shows that the addition of the fifth mode does not significantly improve the identification, indeed, passing from four to five modes, the damage index exhibits high values at the central and upstream beam, thus reducing the readability of the correct damage location, compare Figs. 13 and 14. The reason for this trend is probably due to the low sensitivity of the fifth vibration mode to damage (as shown in [9]), that makes quite unreliable the values of the FRFs—hence the values of the damage index—in the corresponding frequency range.

Concerning the last damage configuration $D7$, we recall that it was obtained by introducing a second concentrated damage at the mid-span of the downstream beam (see Fig. 4). In order to check the capability of the IDDM to localize a new

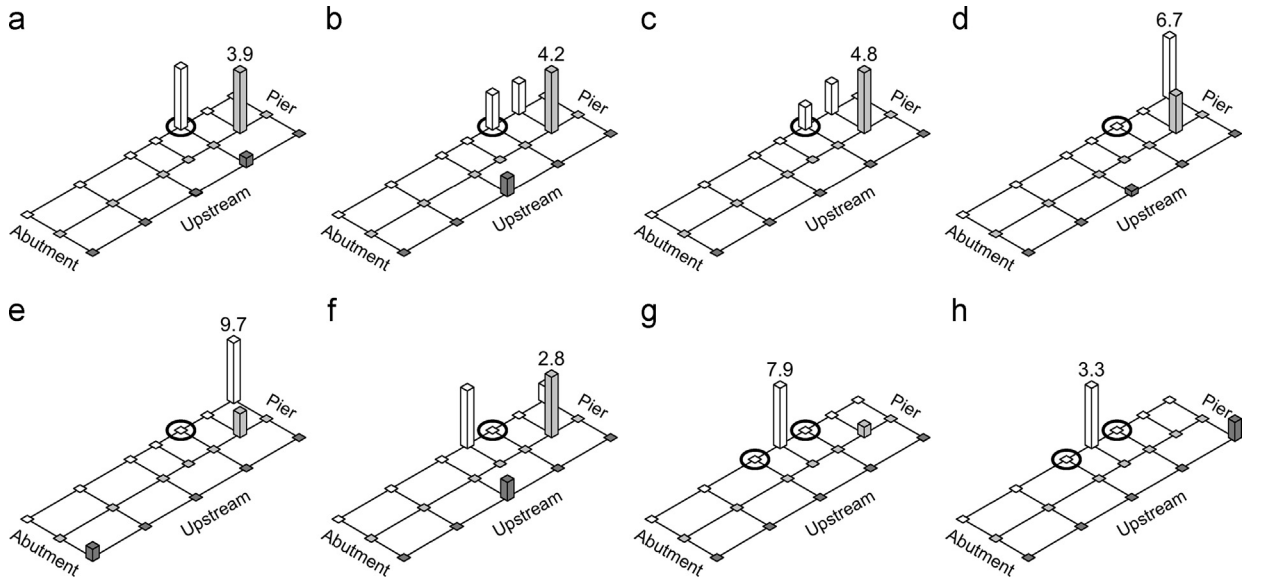

Fig. 11. Damage index D evaluated in the interval 8–15 Hz (first two vibrating modes) from the reference configuration (U) to actual damage configuration: (a) $D1$; (b) $D2$; (c) $D3$; (d) $D4$; (e) $D5$; (f) $D6$; (g) $D7$; (h) from $D6$ to $D7$. Threshold $\nu=1$. Circles denote the actual damage locations.

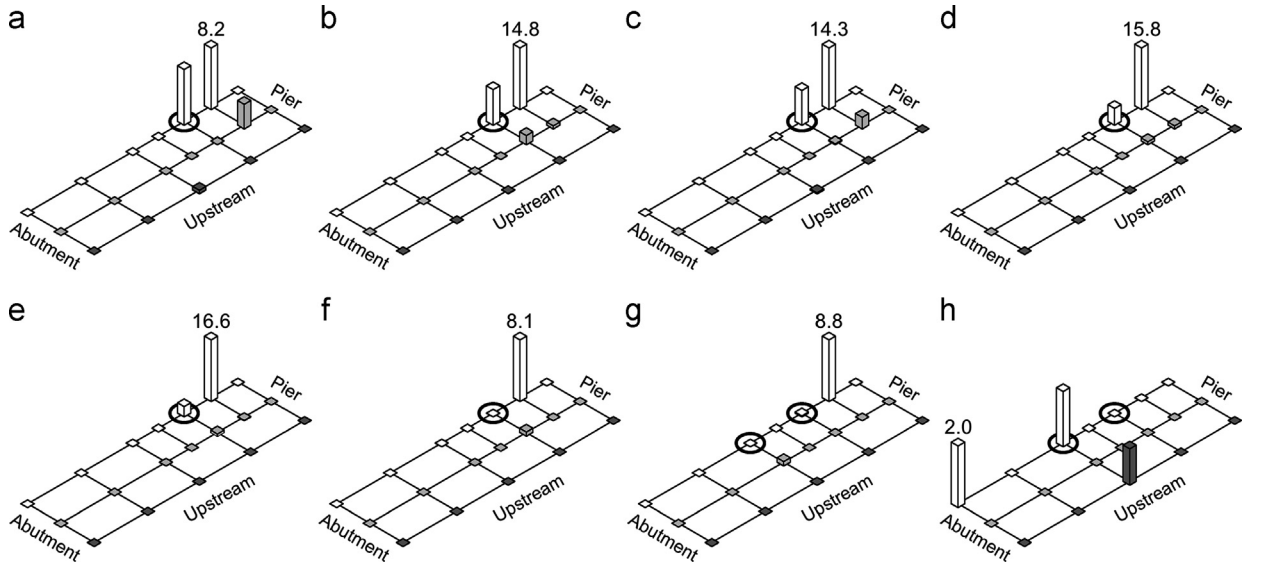

Fig. 12. Damage index D evaluated in the interval 8–28 Hz (first three vibrating modes) from the reference configuration (U) to actual damage configuration: (a) $D1$; (b) $D2$; (c) $D3$; (d) $D4$; (e) $D5$; (f) $D6$; (g) $D7$; (h) from $D6$ to $D7$. Threshold $\nu=1$. Circles denote the actual damage locations.

damage starting from a configuration already damaged (i.e., D6), the IDDM was applied to identify configuration $D7$ assuming configuration $D6$ as the reference one. Results show that, when more than two modes are considered, the correct damaged section is always detected, although some false alarms occur when three or less vibrating modes are included in the analysis.

For the sake of completeness, the IDDM was also tested to identify the evolution of the damage, that is, to detect a damage scenario starting from a previous damaged configuration. In brief, it turns out that the method gives a clear indication of the occurrence of the damage only when the configuration to be identified is $D7$, for any choice of the starting configuration. The method fails in other circumstances. A possible justification of this behavior is connected with the main hypothesis underlying the IDDM, that is, the assumption that a concentrated damage reflects in a loss of spatial regularity of the vibrational profile of a structure, compared with a reference state. The results seem to suggest that a significant loss of spatial regularity occurs essentially at the beginning of the damage process, and, therefore, it cannot be detected between successive damage stages in the case of a single concentrated damage. This is confirmed by the good results obtained in

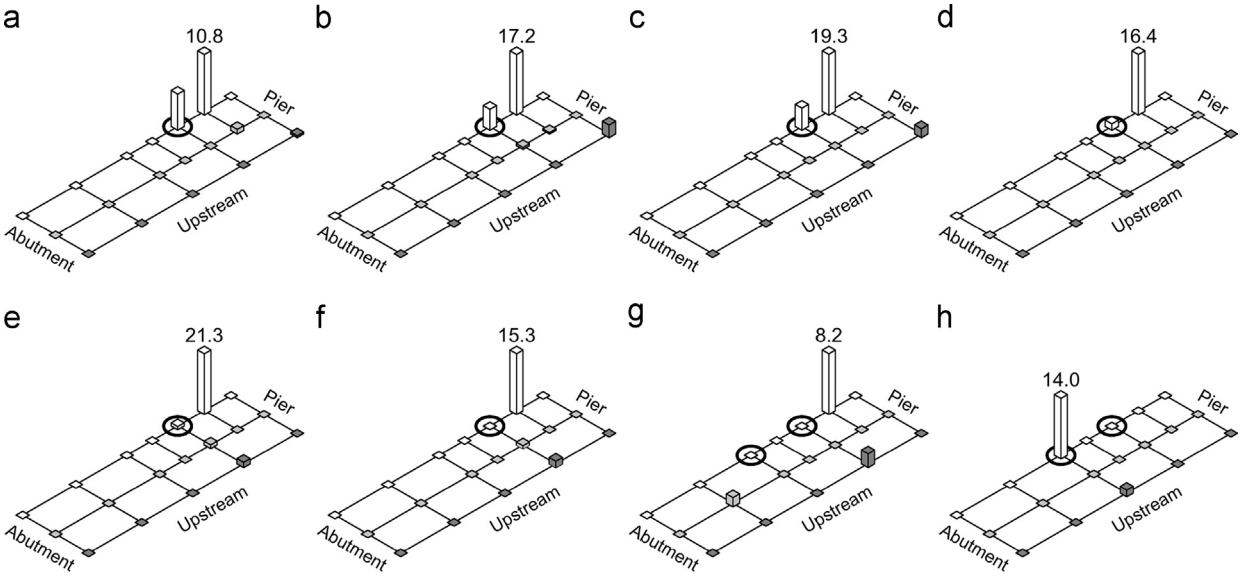

Fig. 13. Damage index D evaluated in the interval 8–38 Hz (first four vibrating modes) from the reference configuration (U) to actual damage configuration: (a) $D1$; (b) $D2$; (c) $D3$; (d) $D4$; (e) $D5$; (f) $D6$; (g) $D7$; (h) from $D6$ to $D7$. Threshold $\nu=1$. Circles denote the actual damage locations.

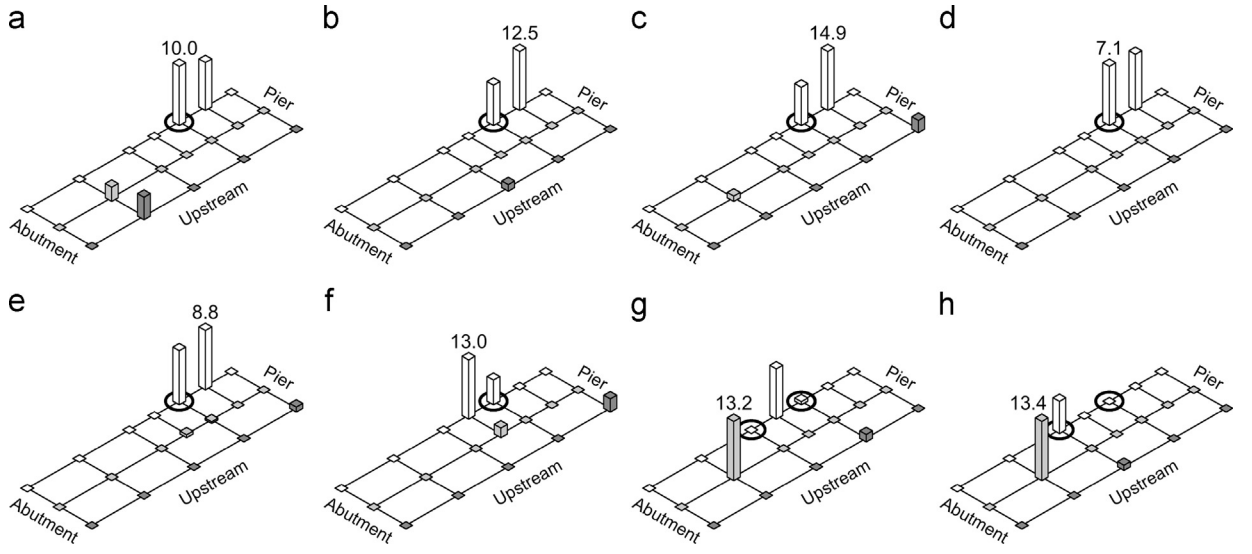

Fig. 14. Damage index D evaluated in the interval 8–50 Hz (first five vibrating modes) from the reference configuration (U) to actual damage configuration: (a) $D1$; (b) $D2$; (c) $D3$; (d) $D4$; (e) $D5$; (f) $D6$; (g) $D7$; (h) from $D6$ to $D7$. Threshold $\nu=1$. Circles denote the actual damage locations.

identifying damage D7 occurring at a different position with respect to damages $D1$–$D6$, thus inducing a loss of spatial regularity with respect to each of the former configurations (both damaged and undamaged).

We conclude this section by repeating the above analysis for different choices of the set of instrumented points. In a first stage, all the instrumented points are considered in the evaluation of the damage index. In general terms, a larger amount of data improves the identification and the result of damage localization turns out to be better than before, both for $\nu=1$ and $\nu=2$, as it is confirmed, by way of an example, by Figs. 15 and 16 ($\nu=2$) in the case that first two or first four vibration modes are taken into account. In particular, false alarms located far from the actual damage position are reduced in number and, moreover, the performance of the choice $\nu=2$ is now comparable to that resulting from taking $\nu=1$. Finally, the above results are compared with those obtained from a less refined mesh. Figs. 17 and 18 ($\nu=1$) show, in particular, the damage index value when the sensors A10, A11, A15 and A16, which are close to the damaged area, are not included in calculations. Comparing with Figs. 13 and 14, the results of identification are quite stable, even if the quality becomes worse when the fifth vibration mode is considered, probably because of its low sensitivity to damage, as it was mentioned above.

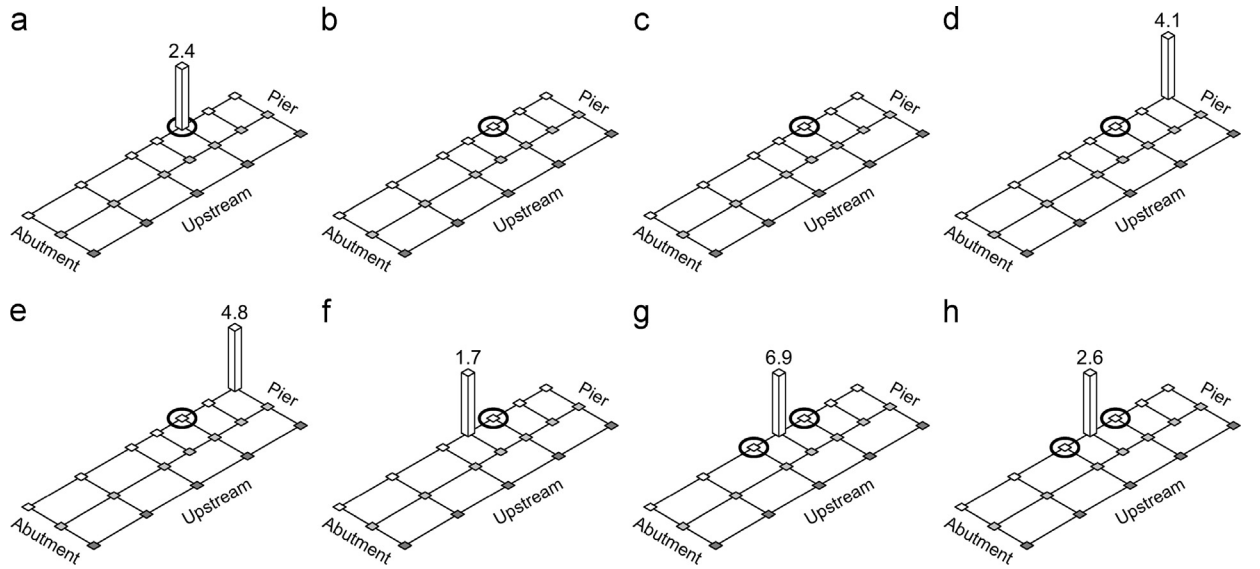

Fig. 15. Damage index D evaluated in the interval 8–15 Hz (first two vibrating modes) from the reference configuration (U) to actual damage configuration: (a) $D1$; (b) $D2$; (c) $D3$; (d) $D4$; (e) $D5$; (f) $D6$; (g) $D7$; (h) from $D6$ to $D7$. Threshold $\nu=2$ and all the instrumented points are considered in the evaluation of the damage index. Circles denote the actual damage locations.

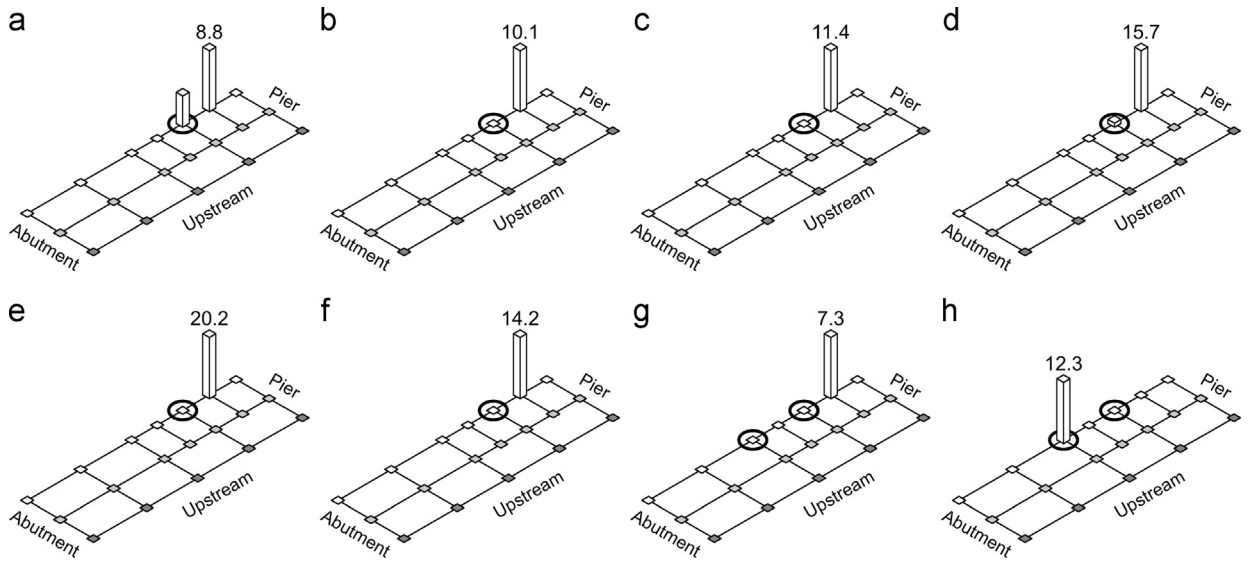

Fig. 16. Damage index D evaluated in the interval 8–38 Hz (first four vibrating modes) from the reference configuration (U) to actual damage configuration: (a) $D1$; (b) $D2$; (c) $D3$; (d) $D4$; (e) $D5$; (f) $D6$; (g) $D7$; (h) from $D6$ to $D7$. Threshold $\nu=2$ and all the instrumented points are considered in the evaluation of the damage index. Circles denote the actual damage locations.

4.2. A couple of variants

A first variant of the method consists in assuming the interpolation error $E(z_l,f_i)$ given as the absolute value of the difference between the modulus of the recorded and interpolated FRFs, namely

$$E(z_l,f_i)=\left|\left|H_R(z_l,f_i)\right|-\left|H_S(z_l,f_i)\right|\right|, \tag{8}$$

where z_l is the location considered and f_i the ith frequency value, see also [23]. This choice obviously entails a reduction in input information, as the phase data are not used, and, therefore, it is expected that identification results could be affected compared to the case in which all the information on FRF is known. It is worth noticing that choice (8) is of interest in applications, since it leads to a simpler calculation of the damage index and, ultimately, to more expeditious diagnostic analysis. Calculations analogous to those developed in the previous section were repeated under assumption (8). Corresponding results (with damage index evaluated separately for each alignment of the sensors) are summarized in Figs. 19–22, and should be compared with those shown in Figs. 11–14. The quality of the identification is comparable,

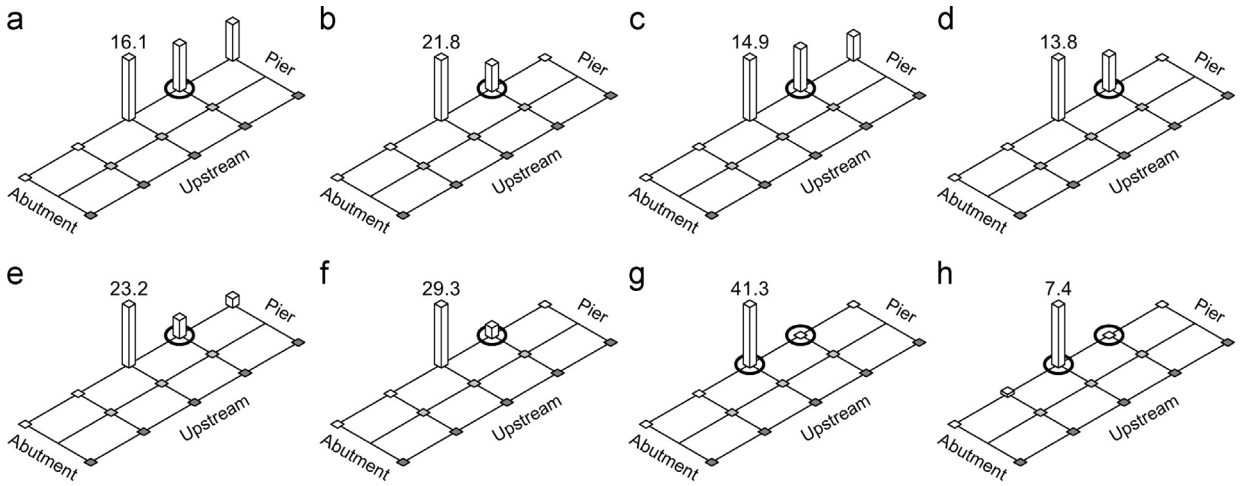

Fig. 17. Damage index D evaluated in the interval 8–38 Hz (first four vibrating modes) from the reference configuration (U) to actual damage configuration: (a) $D1$; (b) $D2$; (c) $D3$; (d) $D4$; (e) $D5$; (f) $D6$; (g) $D7$; (h) from $D6$ to $D7$. Threshold $\nu=1$ and all the instrumented points, with the exception of the sensors A10, A11, A15 and A16, are considered in the evaluation of the damage index. Circles denote the actual damage locations.

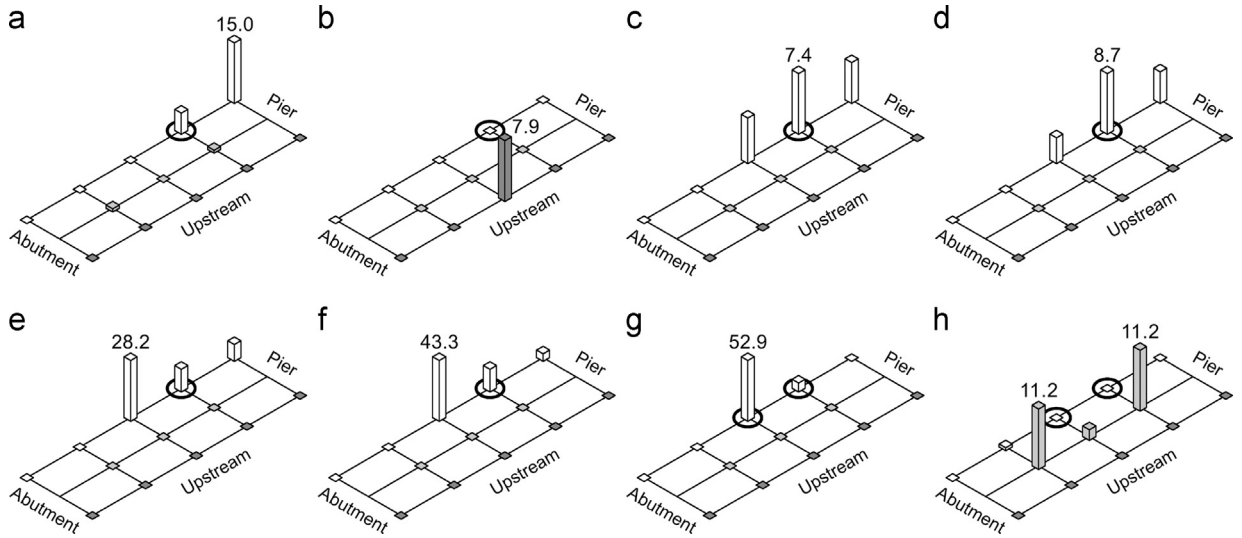

Fig. 18. Damage index D evaluated in the interval 8–50 Hz (first five vibrating modes) from the reference configuration (U) to actual damage configuration: (a) $D1$; (b) $D2$; (c) $D3$; (d) $D4$; (e) $D5$; (f) $D6$; (g) $D7$; (h) from $D6$ to $D7$. Threshold $\nu=1$ and all the instrumented points, with the exception of the sensors A10, A11, A15 and A16, are considered in the evaluation of the damage index. Circles denote the actual damage locations.

although now there is a more pronounced dispersion of the index values, in particular when the first three or the first five modes of vibration are included in the analysis.

In a second stage, the sensitivity of the IDDM to a different extension of experimental FRFs outside the measuring ranges has been investigated. In particular, the analytical expression of the FRF (in *receptance* form)

$$H_{kl}(s)=\sum_{r=1}^{N}\frac{A_{kl}^{(r)}}{s-s_r}+\frac{\overline{A}_{kl}^{(r)}}{s-\overline{s}_r},\quad A_{kl}^{(r)}=\frac{u_k^{(r)}u_l^{(r)}}{2ip_{rd}m_r}, \tag{9}$$

obtained in [9] as the result of a specific curve fitting technique applied around the resonances of the first five modes of vibration has been used. In Eqs. (9), $N=5$; $s=i\omega$ is the frequency variable; $s_r=-\xi_r p_r+ip_{rd}$ is the complex pole of the rth vibration mode, p_r and $p_{rd}=p_r\,(1-\xi_r^2)^{1/2}$ being the undamped and damped circular frequency for mode r, respectively; $u_l^{(r)}$ is the lth component of the rth mode shape; and $m_r=\Sigma_{k,l=1}^{L}M_{kl}u_k^{(r)}\,u_l^{(r)}$, where M_{kl} is the (k,l)-component of the mass matrix and L is the number of the monitored degrees of freedom. The complex conjugate of a number is denoted by an overbar.

As an example, Fig. 23 shows the trends of the FRF analogous to those illustrated in Fig. 6. Despite the high accuracy of the local reconstruction of experimental FRFs, see Table 2 in [9], significant jump discontinuities of the FRF magnitude occur at boundary points between measured and reconstructed FRFs. It is worth noticing that, in order to ensure an accurate estimation of modal parameters associated with a particular mode of vibration, a curve fitting technique including the

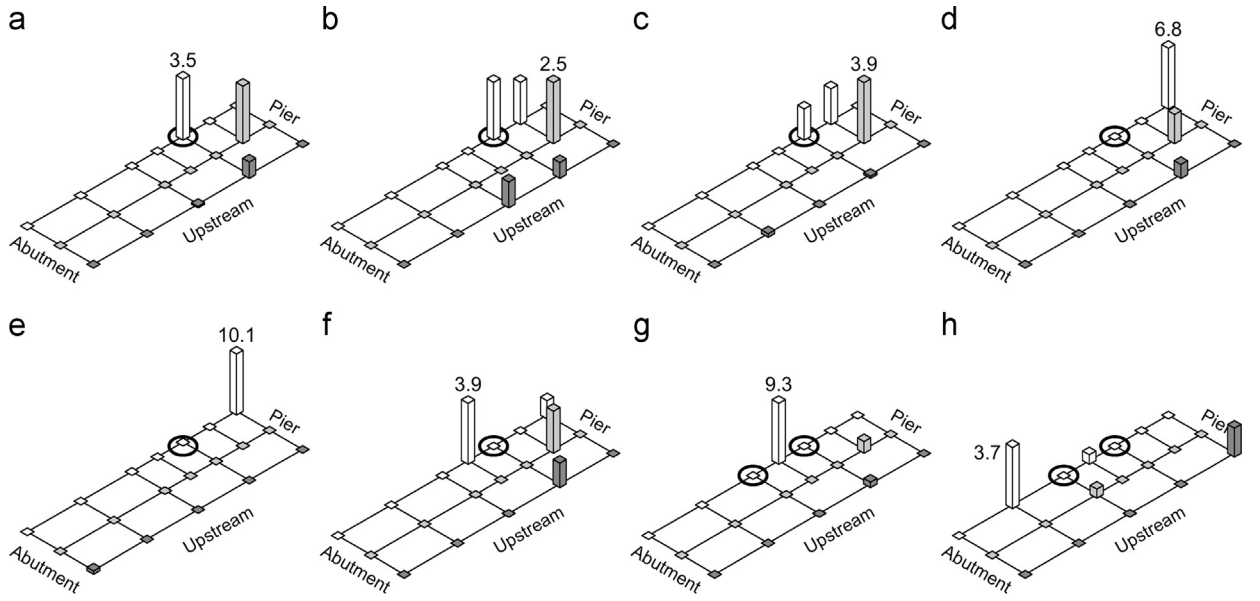

Fig. 19. Damage index D evaluated according to Eq. (8) in the interval 8–15 Hz (first two vibrating modes) from the reference configuration (U) to actual damage configuration: (a) $D1$; (b) $D2$; (c) $D3$; (d) $D4$; (e) $D5$; (f) $D6$; (g) $D7$; (h) from $D6$ to $D7$. Threshold $\nu = 1$. Circles denote the actual damage locations.

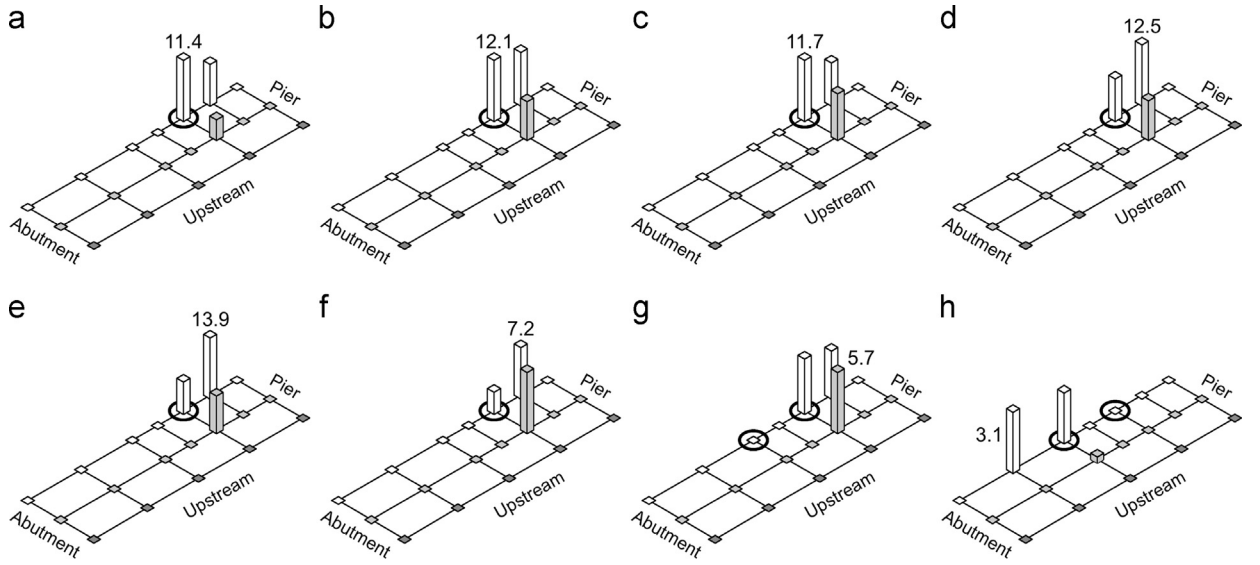

Fig. 20. Damage index D evaluated according to Eq. (8) in the interval 8–28 Hz (first three vibrating modes) from the reference configuration (U) to actual damage configuration: (a) $D1$; (b) $D2$; (c) $D3$; (d) $D4$; (e) $D5$; (f) $D6$; (g) $D7$; (h) from $D6$ to $D7$. Threshold $\nu = 1$. Circles denote the actual damage locations.

contribution of adjacent vibration modes was implemented in [9]. The method allowed for an excellent repeatability in both the estimation of modal parameters and the local FRF reconstruction (as it is shown, by way of an example, in Fig. 24), but did not guarantee a comparable accuracy in global FRF reconstruction by extrapolation from measuring intervals to the entire frequency range 8–50 Hz. In this regard, it should be noticed that having even few points outside the resonance neighborhoods, would have been probably enough to provide stable reconstruction of the FRF in a wide frequency range.

The results of the IDDM are summarized in Figs. 25 and 26 for damage index evaluated separately for each alignment of sensors. Generally speaking, high values of the damage index (evaluated according to Eq. (8)) are found in correspondence to the actual position of the damage. At the same time, however, several false alarms occur in incorrect positions and, moreover, the accuracy of damage localization does not improve when an increasing number of vibration modes is taken into account. Overall, the quality of the identification results turns out to be worse than the case in which the FRFs were extended outside of the measurement intervals by linear interpolation. The reason for this can be attributed to the presence of the jump discontinuities in reconstructing the FRF terms by the analytical extension (9). Indeed, these singularities may

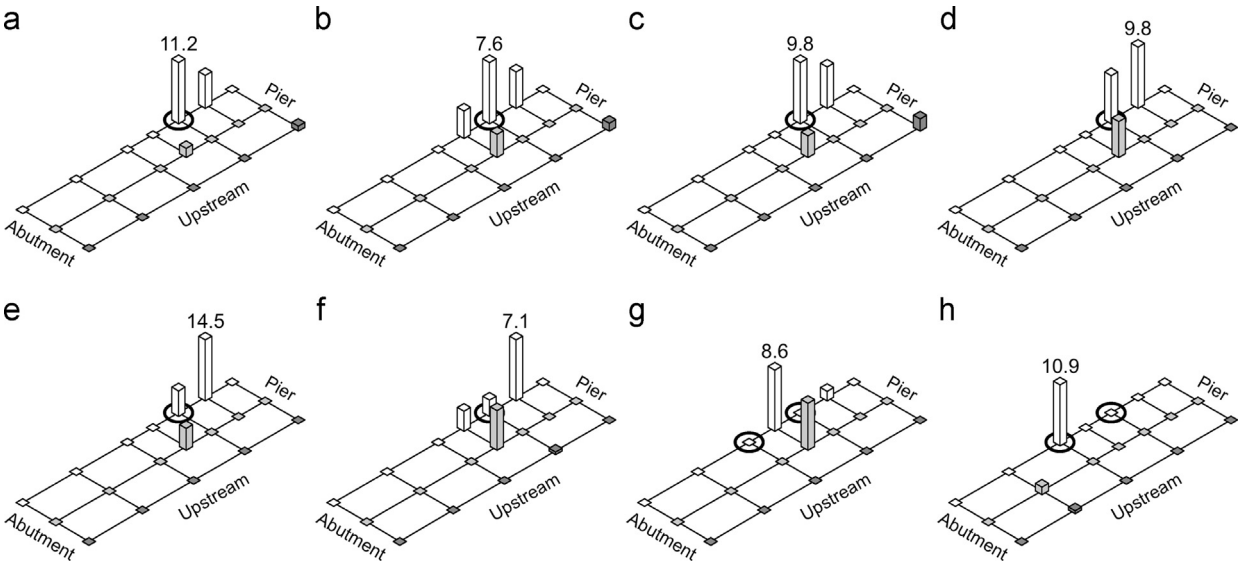

Fig. 21. Damage index D evaluated according to Eq. (8) in the interval 8–38 Hz (first four vibrating modes) from the reference configuration (U) to actual damage configuration: (a) $D1$; (b) $D2$; (c) $D3$; (d) $D4$; (e) $D5$; (f) $D6$; (g) $D7$; (h) from $D6$ to $D7$. Threshold $\nu=1$. Circles denote the actual damage locations.

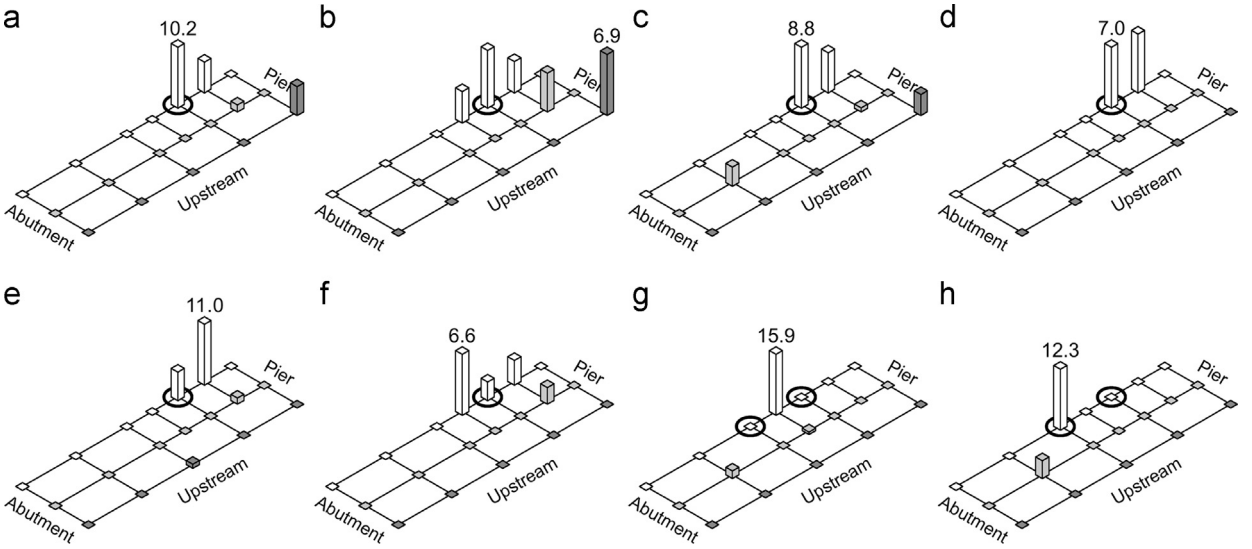

Fig. 22. Damage index D evaluated according to Eq. (8) in the interval 8–50 Hz (first five vibrating modes) from the reference configuration (U) to actual damage configuration: (a) $D1$; (b) $D2$; (c) $D3$; (d) $D4$; (e) $D5$; (f) $D6$; (g) $D7$; (h) from $D6$ to $D7$. Threshold $\nu=1$. Circles denote the actual damage locations.

develop at different frequency values from one damage configuration to another, with the consequence of altering the spatial trend of the interpolation error, and, ultimately, to mask the real effect of the structural damage on FRF data.

4.3. A comparison with the Modal Curvature Method

A comparison between the above results and those obtained by adapting the Modal Curvature Method (MCM) is discussed in this section. For reader convenience, the main idea of the MCM is briefly recalled in the sequel. We refer to [9] for more details on damage localization in the Dogna Bridge via the MCM and to [15] for the first application of the MCM on a full-scale damaged bridge.

Following the approach presented in [9], let us denote by $0=x_0<x_1<\ldots<x_N=L$ the measurement points along a given longitudinal beam. This decomposition of the interval $[0,L]$ will be denoted by δ. A cubic spline function $f\delta$ associated with the decomposition δ is a C^2-function in $[0,L]$ that coincides with a third order polynomial on every subinterval $[x_i, x_{i+1}]$, $i=0,1,\ldots,N-1$. Let $\mathbf{y}^{(\mathbf{r})}=(y_0^{(r)},y_1^{(r)},\ldots, y_N^{(r)})$ be the restriction of the rth normalized mode of the bridge to the set of measurement points belonging to the beam. A cubic spline function $f\delta(\mathbf{y}^{(\mathbf{r})}, \cdot)$ defined on $[0,L]$ and such that $f\delta(\mathbf{y}^{(\mathbf{r})}, x_i)= y_i^{(r)}$, $i=0,1,\ldots,N$, is called *natural* cubic spline function if $f\delta''(\mathbf{y}^{(\mathbf{r})}, 0)=0=f\delta''(\mathbf{y}^{(\mathbf{r})}, L)$. Note that these conditions are certainly verified at the ends

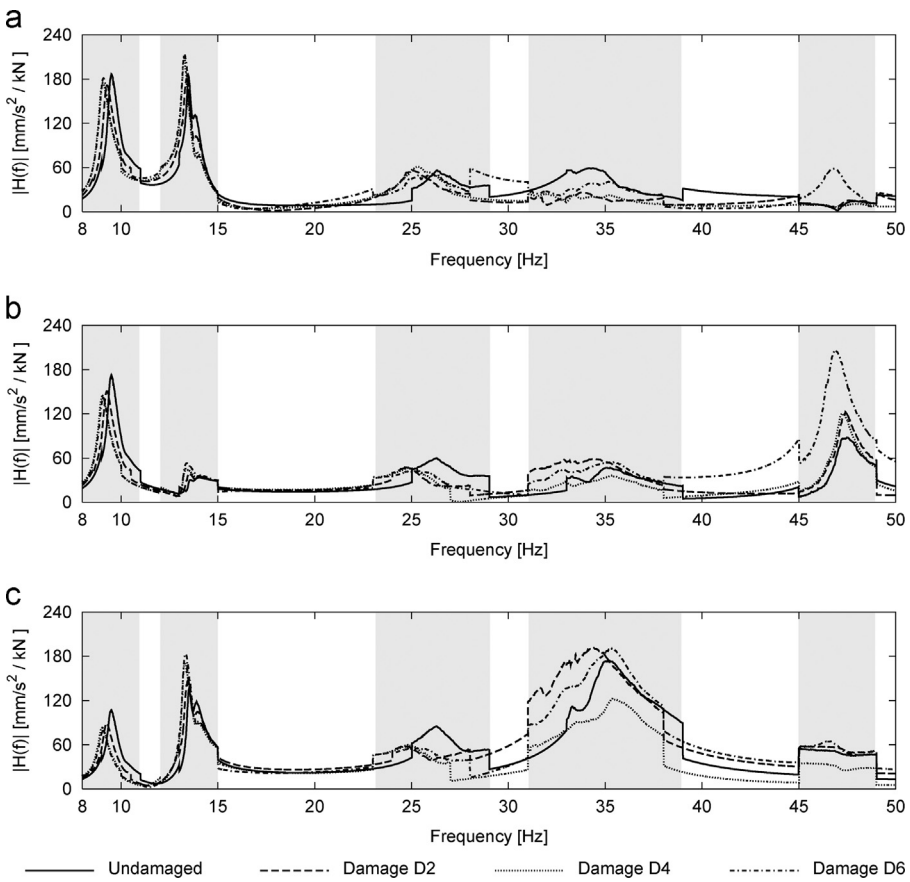

Fig. 23. FRF amplitude at locations A10 (a), A11 (b) and A14 (c) obtained by analytic extension (9) outside the measured intervals (in gray).

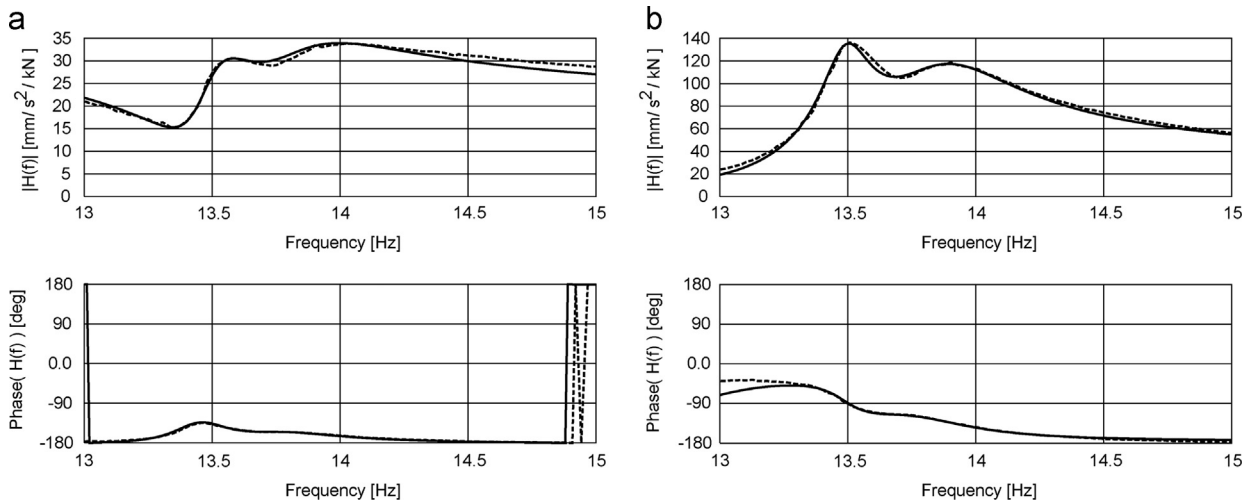

Fig. 24. Example of comparison between analytical (continuous line) and experimental (dotted line) FRF in a neighborhood of the second natural frequency. FRF at locations A11 (a) and A14 (b).

of longitudinal beams of the Dogna Bridge because of simple support end conditions. Under the above assumptions, it is possible to show that there exists a unique natural cubic spline function $f\delta(\mathbf{y}^{(\mathbf{r})}, \cdot)$ associated to the decomposition δ and data $\mathbf{y}^{(\mathbf{r})}$. An efficient algorithm for reconstructing the natural spline function is also available, see [9].

Some results of the MCM applied to the Dogna Bridge are summarized in Figs. 27 and 28. In these figures, the variation of the modal curvature of the first and second normalized (with respect to the mass matrix of the undamaged state) vibrating

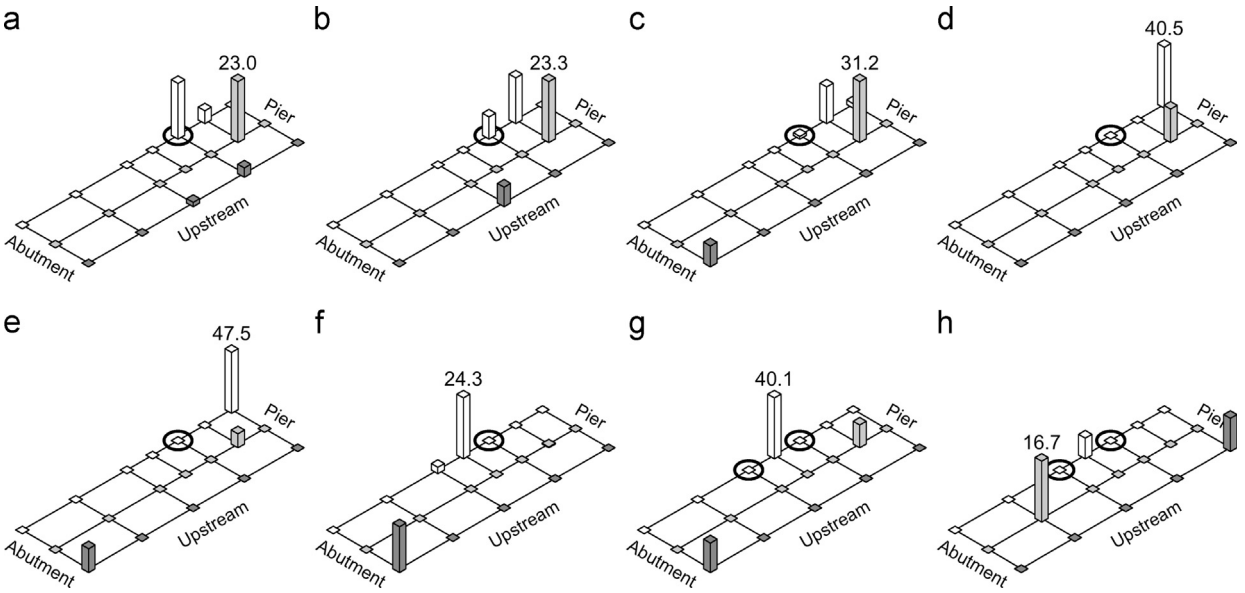

Fig. 25. Damage index D evaluated according Eq. (8) and by using the analytical extension (9) in the interval 8–15 Hz (first two vibrating modes) from the reference configuration (U) to actual damage configuration: (a) $D1$; (b) $D2$; (c) $D3$; (d) $D4$; (e) $D5$; (f) $D6$; (g) $D7$; (h) from $D6$ to $D7$. Threshold $\nu = 1$. Circles denote the actual damage locations.

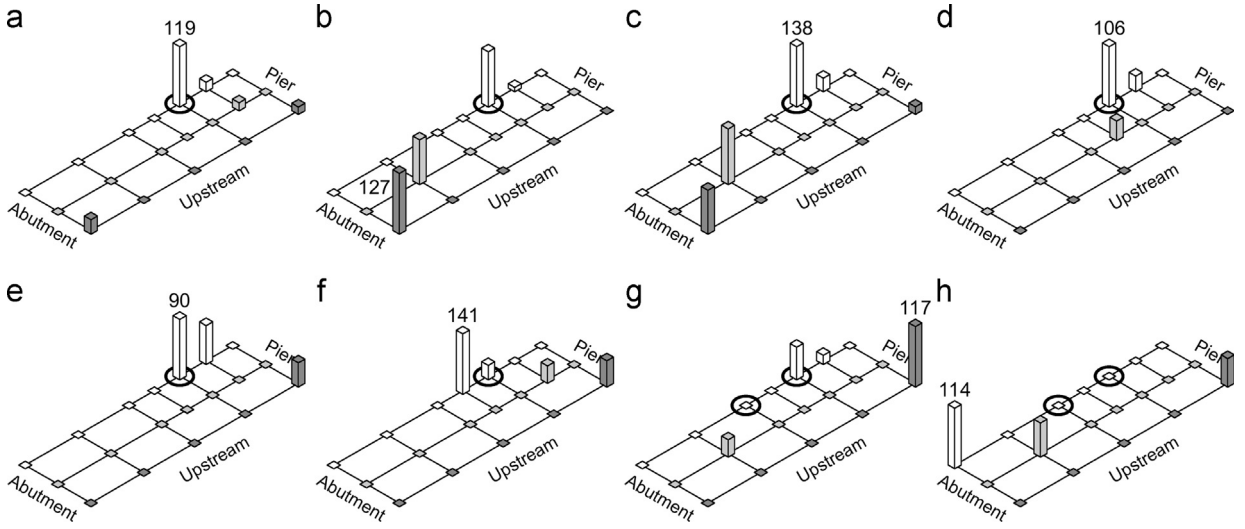

Fig. 26. Damage index D evaluated according Eq. (8) and by using the analytical extension (9) in the interval 8–38 Hz (first four vibrating modes) from the reference configuration (U) to actual damage configuration: (a) $D1$; (b) $D2$; (c) $D3$; (d) $D4$; (e) $D5$; (f) $D6$; (g) $D7$; (h) from $D6$ to $D7$. Threshold $\nu = 1$. Circles denote the actual damage locations.

mode from the undamaged configuration to a damaged configuration are represented, respectively. In particular, in order to facilitate the comparison with the results obtained by the IDDM, Figs. 27 and 28 show the absolute value of the changes of the modal curvatures evaluated at the nodes of the spatial mesh used in the experiments. Fig. 27 clearly shows a significant increase of the first modal curvature on the downstream beam, near the third-span/fourth-span side-pier. This indication is confirmed also by the appearance of changes, this time more limited, on the same region of the central beam, whereas the modal curvature of the upstream beam remains approximately constant for the various damaged configurations. Similar information can be extracted from the second mode (see Fig. 28). It can be shown that less accurate information is provided by the third vibration mode, probably because of poor spatial resolution of the measuring points. From the variations of modal curvature it is also possible to appreciate the increased severity of the damage from configuration $D1$ to $D6$. On the contrary, detection and localization of damage $D7$ from damage configuration $D6$ seems not be possible, probably because of the small sensitivity to damage of lower vibration modes of the bridge to this damage scenario.

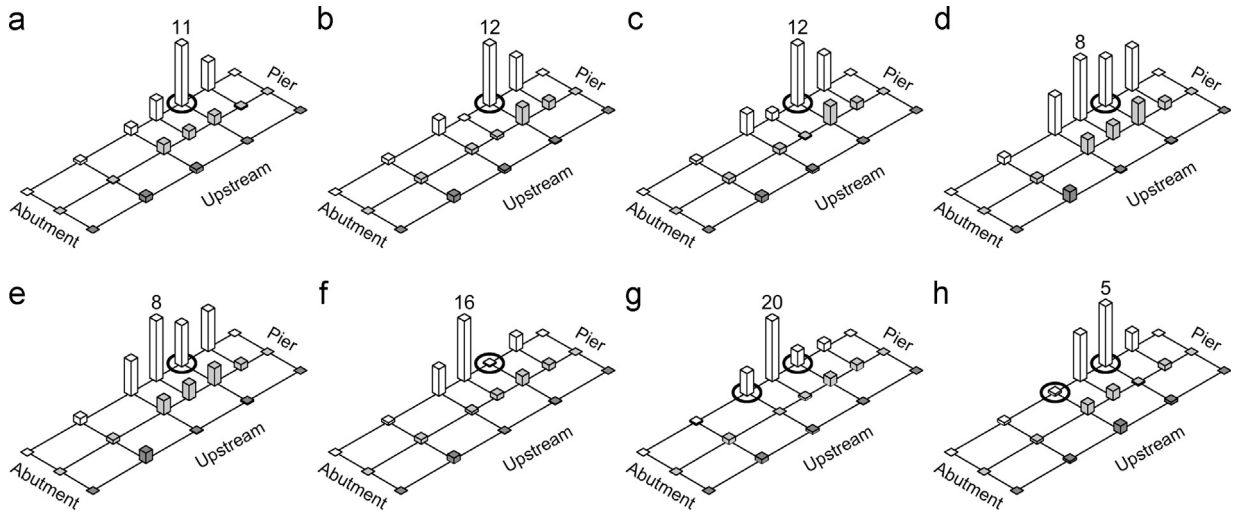

Fig. 27. Absolute value of the modal curvature variation of the first (normalized vibration mode) from the undamaged configuration (*U*) to actual damage configuration: (a) *D*1; (b) *D*2; (c) *D*3; (d) *D*4; (e) *D*5; (f) *D*6; (g) *D*7; (h) from *D*6 to *D*7. Circles denote the actual damage locations.

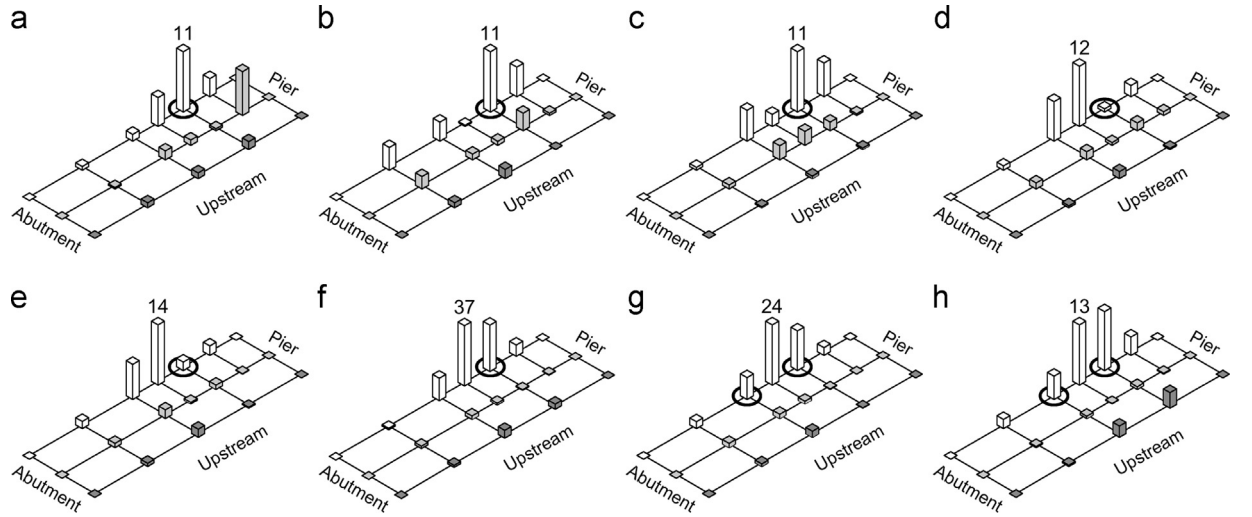

Fig. 28. Absolute value of the modal curvature variation of the second (normalized vibration mode) from the undamaged configuration (*U*) to actual damage configuration: (a) *D*1; (b) *D*2; (c) *D*3; (d) *D*4; (e) *D*5; (f) *D*6; (g) *D*7; (h) from *D*6 to *D*7. Circles denote the actual damage locations.

5. Conclusions

An application of the Interpolation Damage Detection Method for the localization of damage in a single-span reinforced concrete bridge has been presented in this paper. The damage consists of a series of notches made on a lateral beam to simulate the effect of incremental concentrated damage. Experimental data are the frequency response functions measured around the first five resonant frequencies on a grid of points on the bridge deck. The IDDM is essentially based on a comparison between the FRFs before and after the occurrence of a structural damage, and on the determination of an index that takes into account the loss of spatial regularity of the vibrational profile of a structure, compared with a reference (e.g., undamaged) state, induced by a localized damage. The method has the advantage of not requiring the development of a numerical model of the vibrating system, since it works directly with the experimental data.

Among other aspects, the analysis presented in this paper allowed to point out some features of the IDDM not yet showed in previous applications. A first aspect worth of mention is the stability of the method to different extension/extrapolation from the (narrow) frequency intervals in which the FRF data is available to larger frequency range. Our results confirm that a linear interpolation of the measured values between adjacent measured intervals should be sufficient. A second aspect highlighted by the present application, is the ability of the IDDM to localize damage whenever a network of sensors dense enough is deployed. In our experience, five in-span measurements are enough. In particular, our results show that if sensors are deployed along more than one alignment in the longitudinal direction of the bridge, then the diagnostic method allows not only to detect the position of damage along this direction but also to correctly locate the damage on the

transverse direction. Finally, concerning the ability of the IDDM in identifying the evolution of the damage, our results suggest that this can be done, provided that the severity of damage to be identified corresponds to a not negligible additional localized loss of spatial regularity of the vibrational amplitude profile with respect to the previous configurations of the structure.

Overall, the results of this paper confirm that the IDDM can be considered a useful tool for a preliminary localization of structural damage in full-scale bridges. However, there are still some open problems connected with the proposed diagnostic method. The accuracy of the FRF measurements, the typology of the damage and the features of the Dogna Bridge were probably decisive factors for the success of the identification. In other contexts, the sensitivity of the problem to the accuracy and completeness of the data, and the complexity of the system may play an important role. In addition, the IDDM is currently based on the assumption that an increase of the interpolation error at one instrumented location between reference and damaged state can be considered as an indicator of the existence of structural damage close to the location where the change is detected. It would be worth to considering the mathematical basis of this conjecture, even for simple vibrating systems, and proving rigorously that the damage index D can effectively provide an indication on the existence and location of the degradation. All these problems require further investigation, both of theoretical and experimental character.

Acknowledgment

The work of A. Morassi is partially supported by the University Carlos III of Madrid—Banco de Santander Chairs of Excellence Programme for the 2013–2014 Academic Year. A. Morassi wishes to thank the colleagues of the University Carlos III of Madrid, especially Professors L. Rubio and J. Fernández-Sáez, for the warm hospitality at the Department of Engineering Mechanics.

References

[1] T. Toksoy, A.E. Aktan, Bridge-condition assessment by modal flexibility, Exp. Mech. 34 (1994) 271–278.
[2] A. Teughels, G. De Roeck, Structural damage identification of the highway bridge Z24 by FE model updating, J. Sound Vib. 278 (2004) 589–610.
[3] P.J.S. Cruz, R. Salgado, Performance of vibration-based damage detection methods in bridges, Comput.-Aided Civ. Infrastruct. Eng. 24 (2009) 62–79.
[4] F. Necati Catbas, M. Gul, J.L. Burkett, Conceptual damage-sensitive features for structural health monitoring: Laboratory and field demonstrations, Mech. Syst. Signal Process. 22 (2008) 1650–1669.
[5] F. Magalhaes, A. Cunha, E. Caetano, Vibration based structural health monitoring of an arch bridge: From automated OMA to damage detection, Mech. Syst. Signal Process. 28 (2012) 212–228.
[6] M. Kato, S. Shimada, Vibration of PC bridge during failure process, J. Struct. Eng. ASCE 112 (1986) 1692–1703.
[7] C.R. Farrar, D.A. Jauregui, Comparative study of damage identification algorithms applied to a bridge: I. Experiment, Smart Mater. Struct. **7** (1998) 704–719.
[8] J. Maeck, B. Peeters, G. De Roeck, Damage identification on the Z24 bridge using vibration monitoring, Smart Mater. Struct. 10 (2001) 512–517.
[9] M. Dilena, A. Morassi, Dynamic testing of a damaged bridge, Mech. Syst. Signal Process. 25 (2011) 1485–1507.
[10] H.J. Salane, J.W. Baldwin Jr., Identification of modal properties of bridges, J. Struct. Eng. ASCE 116 (1990) 2008–2021.
[11] M. Dilena, A. Morassi, M. Perin, Dynamic identification of a reinforced concrete damaged bridge, Mech. Syst. Signal Process. 25 (2011) 2990–3009.
[12] D.F. Mazurek, J.T. De Wolf, Experimental study of bridge monitoring technique, J. Struct. Eng. ASCE 116 (1990) 2532–2549.
[13] F. Necati Catbas, D.L. Brown, A.E. Aktan, Use of modal flexibility for damage detection and condition assessment: case studies and demonstrations on large structures, J. Struct. Eng. ASCE 132 (2006) 1699–1712.
[14] A.K. Pandey, M. Biswas, M.M. Samman, Damage detection from changes in curvature mode shapes, J. Sound Vib. 145 (1991) 321–332.
[15] M.M.A. Wahab, G. De Roeck, Damage detection in bridges using modal curvatures: application to a real damage scenario, J. Sound Vib. 226 (1999) 217–235.
[16] O. Huth, G. Feltrin, J. Maeck, N. Kilic, M. Motavalli, Damage identification using modal data: experiences on a prestressed concrete bridge, J. Struct. Eng. ASCE 131 (2005) 1898–1910.
[17] R.P.C. Sampaio, N.M.M. Maia, J.M.M. Silva, Damage detection using the frequency response function curvature method, J. Sound Vib. 226 (1999) 1029–1042.
[18] C.P. Ratcliffe, Damage detection using a modified Laplacian operator on mode shape data, J. Sound Vib. 204 (1997) 505–517.
[19] T. Ramesh Babu, A.S. Sekhar, Detection of two cracks in a rotor-bearing system using amplitude deviation curve, J. Sound Vib. 314 (2008) 457–464.
[20] Y. Zhang, S.T. Lie, Z. Xiang, Damage detection method based on operating deflection shape curvature extracted from dynamic response of a passing vehicle, Mech. Syst. Signal Process. 35 (2013) 238–254.
[21] P.F. Pai, S. Jin, Locating structural damage by detecting boundary effects, J. Sound Vib. 231 (4) (2000) 1079–1110.
[22] M.P. Limongelli, Frequency response function interpolation for damage detection under changing environment, Mech. Syst. Signal Process. 24 (2010) 2898–2913.
[23] M.P. Limongelli, The Interpolation Damage Detection Method for frames under seismic excitation, J. Sound Vib. 330 (2011) 5474–5489.
[24] S. Caddemi, A. Morassi, Detecting multiple cracks in elastic beams by static tests, J. Eng. Mech. ASCE 137 (2011) 113–124.
[25] A. Morassi, E. Rosset, S. Vessella, Recent results about the detection of unknown boundaries and inclusions in elastic plates, J. Inverse Ill-Posed Probl. 221 (2013) 311–352.